Intermediate Range Wireless Power Transfer With Segmented Coil Transmitters for Implantable Heart Pumps

Sai Chun Tang, *Senior Member, IEEE*, Tian Le Tim Lun, Ziyan Guo, Ka-Wai Kwok, and Nathan J. McDannold

***Abstract*—In wireless power transfer systems, substantial differences in transmission range and alignment sensitivity can occur when the transmitting coil dimensions are varied. A coil with larger inner and outer diameter was found to provide a wider transmission range and lower alignment sensitivity. Accordingly, we developed a larger coil (24×30 cm^2) designed to be embedded in the back of a vest to power dc pumps for artificial hearts or left ventricular assist devices. To significantly reduce the required transmitting coil voltage, the coil was divided into eight segments with resonant capacitors. The coil was operated at 6.78 MHz and evaluated with a 5.3-cm diameter receiving coil. A circuit model for the energy coupling coils was developed to predict the output power and efficiency. Having a coil separation of 7.7 cm, we measured an output power of 48.2 W and a corresponding energy efficiency higher than 80%. The energy coupling coils were also evaluated with a dc pump in parallel to an additional load representing the power consumed by auxiliary circuits of an implanted heart pump. Experimental results showed that the proposed coil segmentation technique for mid-range wireless energy transfer can significantly reduce the transmitter voltage to a safe level ($\sim$10 V_{rms}).**

***Index Terms*—Artificial heart, implantable medical device, left ventricular assist device (LVAD), mid-range wireless power transfer, segmented coil transmitter.**

I. Introduction

VARYING the dimensions of energy transmitting coils in wireless power transfer systems can lead to substantial differences in transmission range and coil alignment sensitivity. This phenomenon can be easily observed by comparing characteristics of conventional transcutaneous transformers and state-of-the-art mid-range wireless power transfer systems. In transcutaneous transformers, the transmitting coil diameter is typically less than 12 cm [1]–[9], resulting in a transmission range limited to 20 mm [2]–[5], and an allowable lateral misalignment around 10 mm [5], [6]. In applications of mid-range wireless power transfer systems, the relatively larger transmitting coils (e.g., 30 cm) can power implantable devices located virtually anywhere in the body without precise alignment [10]–[16].

Transcutaneous transformers for powering total artificial hearts (TAHs) and left ventricular assist devices (LVADs) have been investigated for decades [1]–[9], [17]–[30]. The transmitting coils are usually wound in a pancake shape with an inner diameter ranging from 20 to 50 mm and an outer diameter of 50 to 120 mm [3], [4], [7], [8], [10], [29]. The separation between the transmitting and receiving coils is usually limited to less than 20 mm in order to maintain a reasonable energy efficiency [3]–[5]. In addition, the transcutaneous transformer is relatively sensitive to misalignment error so that precise coil alignment is required; otherwise, the energy coupling and hence efficiency will be diminished. Since the receiving coil must be implanted under the patient's skin and the implantable heart pump is located relatively deep in the body, a pair of long wires are needed to connect the receiving coil to the implanted device. This arrangement substantially increases the surgical time, complexity, and thus cost. The connection wires can also create reliability issues, particularly when encountering frequent and vigorous patient movement.

Recently, mid-range wireless power transfer approaches for implantable devices have attracted considerable attention because the receiving coil can be located deep in the body and precise coil alignment is not necessary [10]–[16]. These approaches provide flexibility for the integration between the receiving coil and the implanted device without a need for long and unreliable connecting wires. However, the required excitation voltage over the transmitting coil of a mid-range system is conventionally much higher than that for the transcutaneous transformer. For example, in an application that powered a 0.35-W capsule endoscope, an excitation voltage of more than 3-kV was required over the mid-range transmitting coil [10], [11]. In applications with higher power consumption, this voltage will be further demanding. This high voltage requirement is obviously a serious concern in terms of patient safety. Moreover, it increases the manufacturing cost due to the need for bulky electrical insulation of the transmitting coil, as well as the application of high-voltage electronic components in the coil driver. In addition, the system energy efficiency can be drastically reduced because of the excessive dielectric power loss under a high voltage stress [14].

Manuscript received February 29, 2016; revised May 6, 2016; accepted June 10, 2016. Date of publication June 28, 2016; date of current version February 2, 2017. This work was supported in part by the Croucher Foundation and in part by the Research Grants Council of Hong Kong. Preliminary results of this paper were presented at the *2016 IEEE International Workshop on Electromagnetics: Applications and Student Innovation Competition* (iWEM). Recommended for publication by Associate Editor J. M. Rivas Davila.

S. C. Tang and N. J. McDannold are with the Radiology Department, Harvard Medical School, Brigham and Women's Hospital, Boston, MA 02115 USA (e-mail: sct@bwh.harvard.edu; njm@bwh.harvard.edu).

T. L. T. Lun, Z. Guo, and K.-W. Kwok are with the Department of Mechanical Engineering, The University of Hong Kong, Pokfulam, Hong Kong (e-mail: timlun@connect.hku.hk; guoziyan@connect.hku.hk; kwokkw@hku.hk).

Color versions of one or more of the figures in this paper are available online at http://ieeexplore.ieee.org.

Digital Object Identifier 10.1109/TPEL.2016.2584558

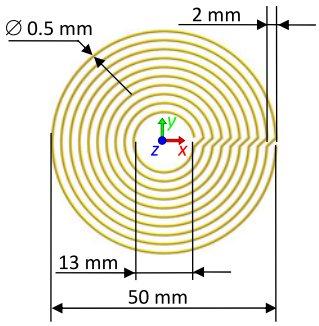

Fig. 1. Dimensions of Coil 1.

A novel low-operating-voltage, mid-range wireless power transfer method was reported previously by Tang *et al.* [13]–[15], who proposed to divide the larger transmitting coil into multiple segments using high-frequency resonant capacitors. The voltage across each segment of the coil is canceled by the adjacent capacitor voltage at the resonant frequency, thus the overall required voltage can be reduced to a safe level, e.g., on the order of 10 V. In this paper, we demonstrate the use of this low-operating-voltage method to a mid-range transmitting coil designed for powering a heart pump. The paper is organized as follows: Section II compares the transmission range and alignment sensitivity of a typical transcutaneous transformer and larger mid-range transmitting coils with different inner diameters. On a basis of these comparison results, a mid-range transmitting coil for the heart pump application is proposed in Section III. Transmission range, alignment sensitivity, and impedance characteristics of the coil are described. Section IV characterizes the energy coupling system with analytical equations and presents the output power and efficiency of the energy coupling coils with different receiving coil locations. In Section V, we present experimental results where energy coupling coils with the proposed design powered a 24-V dc pump that circulated fluid in a simulated circulatory model. Finally, Section VI concludes the paper.

II. Magnetic Field Distributions of Conventional Transcutaneous Transformers and Larger Transmitting Coils

A. Conventional Transcutaneous Transformer Transmitting Coils

In applications of implantable TAH and LVAD, the diameter of the energy transmitting coil in a transcutaneous transformer typically ranges from 5 to 12 cm. The allowable separation between the transmitting and receiving coils is less than 2 cm, and the lateral misalignment tolerance is less than 1 cm. Fig. 1 shows a representative 5-cm transmitting coil (Coil 1), which is made of 10 concentric circular windings connected in series. The coil parameters are listed in Table I. The magnetic field intensity (*H*-field) of each winding in the axial direction H_z can be deduced by (1), as described elsewhere [31]. The overall *H*-field of the 10-turn coil can be obtained by summing the *H*-field generated by all the windings. In this case, which takes advantage of placing the energy transmitting and receiving coils in parallel, we will primarily be interested in the z-component of the *H*-field

$$H_z = \frac{I}{2\pi}\frac{1}{\sqrt{(a+x)^2+z^2}}\left[K(k)+\frac{a^2-x^2-z^2}{(a-x)^2+z^2}E(k)\right] \tag{1}$$

where $K(k)$ and $E(k)$ are complete elliptic integrals of the first and second kind, a is the coil radius, z and x are the distances from the coil center along the coil's axial and radial axes, respectively, I is the winding current, and $k^2 = 4ax/[(a+x)^2+z^2]$.

Finite-element-analysis (FEA) by Ansys Maxwell was also used to simulate the *H*-field. Both the calculated and simulated H_z-field was plotted along the z-axis [see Fig. 2(a)] to investigate the applicable range of the 5-cm transmitting coil. The coil excitation was set to 1 A, i.e., 10 A-turn. At $z = 2$ cm, H_z is reduced by 81.7% and the rate of change of H_z is –8.3%/mm (see Table I). Despite the significant drop and variation of H_z-field, as reported in [4], such a 5-cm transmitting coil can still be adopted to transfer power to a receiving coil with a coil separation of 2 cm. However, this small coil would not be able to efficiently transmit energy deeper than that range. Once the separation along z further increases to 7 cm, H_z drops to 1% of its maximum value.

In addition to the restricted coil separation, the lateral alignment sensitivity of the small transmitting coil can also be noteworthy. Fig. 2(b) depicts H_z along the radial direction at $z = 2$ cm. Comparing with H_z at $x = 0$ cm, H_z drops by 50% at $x = 1.7$ cm and is less than 1% of its maximum when x increases further to 3.5 cm. For this reason, the allowable lateral misalignment of a transcutaneous transformer is generally no more than 1 cm to achieve reasonable power efficiency.

B. Larger Transmitting Coils

Recent reports have demonstrated that larger transmitting coils can transfer energy deep in the body. In an earlier study [12], a single turn 30-cm transmitting coil designed to wrap around the patient's body was developed to power an implanted device placed near the center of the transmitting coil, and the applicable axial range was less than ±3 cm. In other works [10], [11], [13], a pair of Helmholtz coils wrapped around the body was used to generate a very uniform magnetic field over a larger volume to transmit energy to a locomotive capsule endoscope. In the heart pump application, sustaining continuous energy transfer is of importance, and the preferable configuration is to put the larger transmitting coil in parallel to the patient's body, e.g., by embedding the transmitting coil in a vest, chair back, or mattress [30].

In order to investigate the applicable range of a larger transmitting coil placed in parallel to the body, we analyzed the *H*-field distribution of four larger transmitting coils (Coils 2–5) with an outer diameter of 30 cm. The wire diameter of all the coils was 0.5 mm, and the wire separation of Coils 2–4 was 10 mm. Fig. 3 shows the structures of the transmitting coils with parameters listed in Table I. Fig. 4(a) shows the *H*-fields along the z-axis of the four coils with excitation of 10 A-turn. The results show that the *H*-field with a larger inner diameter decreases more slowly than for a smaller inner diameter, and slower still than the 5-cm transmitting coil. For example, with Coil 2, which had the smallest inner diameter, the *H*-field dropped to 50.2% at $z = 7$ cm and 32.6% at $z = 10$ cm, and the rates of change of

TABLE I
PARAMETERS AND CHARACTERISTICS OF THE ENERGY TRANSMITTING COILS

		Coil 1	Coil 2	Coil 3	Coil 4	Coil 5
Inner diameter		1.3 cm	11.9 cm	21.9 cm	27.9 cm	29.9 cm
Outer diameter		5 cm	30 cm			
Wire diameter		0.5 mm				
Number of turns		10	10	5	2	1
H_z along the z-axis (compared with H_z when $z = 0$ cm)	$z = 2$ cm	18.3%	92.3%	96.3%	97.2%	97.4%
	$z = 7$ cm	1.0%	50.2%	67.1%	72.9%	74.4%
	$z = 10$ cm	0.4%	32.6%	48.7%	55.6%	57.5%
Rate of change of H_z along the z-axis	$z = 2$ cm	–8.3%/mm	–0.7%/mm	–0.4%/mm	–0.3%/mm	–0.3%/mm
	$z = 7$ cm	–3.9%/mm	–1.4%/mm	–1.0%/mm	–0.8%/mm	–0.8%/mm
	$z = 10$ cm	–2.9%/mm	–1.4%/mm	–1.1%/mm	–1.0%/mm	–0.9%/mm
Range of x that H_z within 50% of H_z at $x = 0$ when $z = 2$ cm for Coil 1, $z = 10$ cm for Coils 2–5		1.7 cm	10 cm	11.8 cm	13.2 cm	13.7 cm

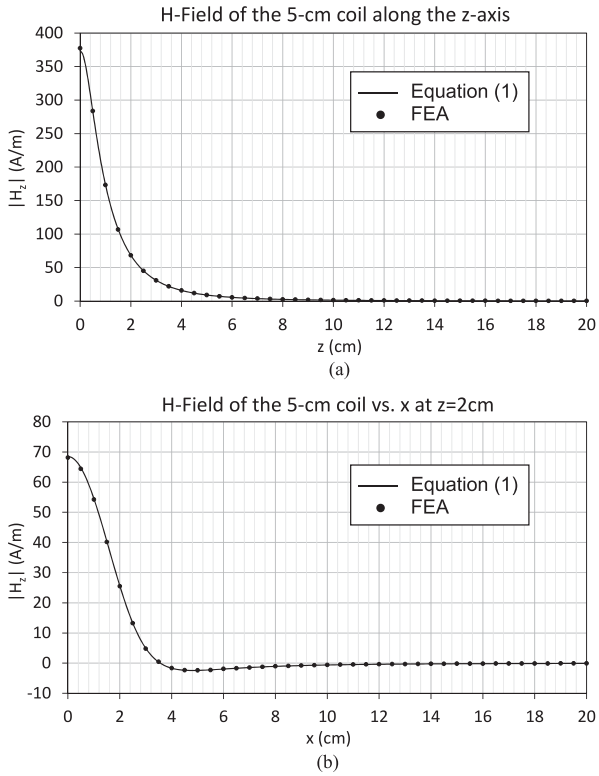

Fig. 2. H_z generated by the 5-cm energy transmitting coil (a) along the z-axis, and (b) versus x at $y = 0$, and $z = 2$ cm.

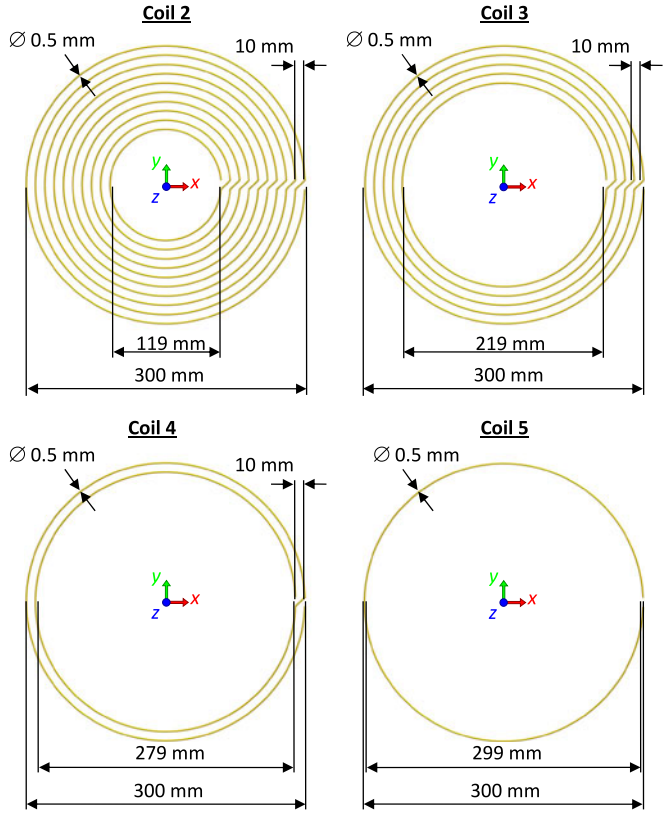

Fig. 3. Dimensions of Coils 2–5 for transmitting energy.

H_z were –1.4%/mm at both positions (see Table I). In contrast, with Coil 5, which had the largest inner diameter, the H-field dropped to 74.4% at $z = 7$ cm and 57.5% at $z = 10$ cm, while the rates of change of H_z were –0.8 and –0.9%/mm, respectively. As a result, increasing the inner and outer diameters of a transmitting coil can transfer energy deeper in the body and reduce the axial alignment sensitivity. It should be noted that although a smaller coil (Coil 1) and a smaller inner diameter coil (Coil 2) can provide a stronger H-field near the coil, their applicable range is much shorter as shown in Figs. 2(a) and 4(a). In heart pump applications, since the pump is implanted deep in the body and it is desired to integrate the receiving coil to the pump to eliminate unreliable long wires connecting the receiving coil to the pump, intermediate-range energy transfer using larger inner and outer diameter transmitting coils is preferred. In this configuration, the receiving coil for an implanted heart pump could be located more than 7 cm from the transmitting coil. For example, for an adult male, the estimated coil separation is around 10 cm depending on the patient's size, so we selected $z = 10$ cm to show the H_z-field along the x-axis [see Fig. 4(b)] for comparing the lateral misalignment sensitivity of the coils with different inner diameters. The range of x where H_z was within 50% of H_z at $x = 0$ are listed in Table I. The results show that the x-range of Coil 5, which had the largest inner diameter, was 37% larger than that of Coil 2 and 8 times larger than that of the 5 cm coil. Accordingly, the results show that increasing the inner and outer diameters can also reduce the lateral alignment sensitivity.

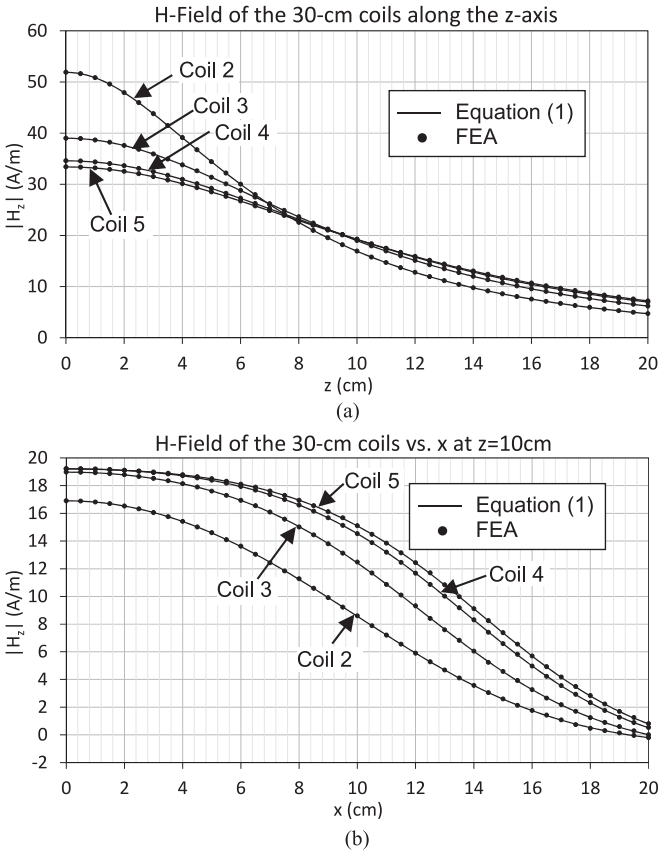

Fig. 4. *H*-field generated by the 30-cm energy transmitting coils (a) along the z-axis, and (b) versus x at $z = 10$ cm when the excitation is 10 A-turn.

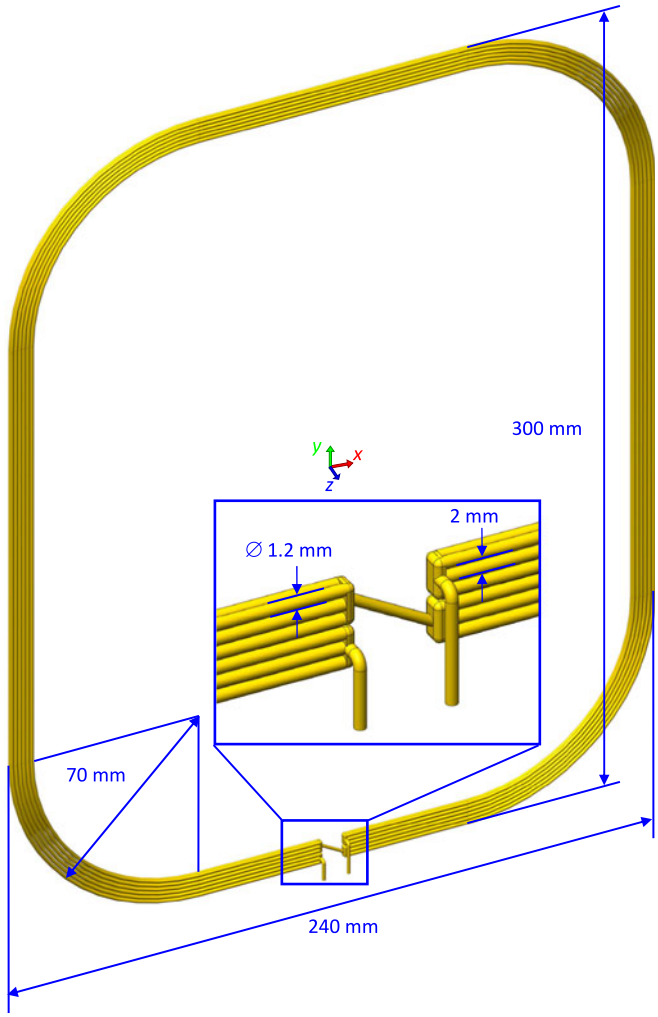

Fig. 5. Three-dimensional drawing of the proposed transmitting coil.

III. Proposed Transmitting Coil

The magnetic field analysis in the previous section suggested that energy transmitting coils with larger inner and outer diameters (Coils 4 and 5) can transmit energy deeper in the body with lower alignment sensitivity. For this reason, we propose a larger transmitting coil designed to power an implanted heart pump that can be embedded in the back of a vest. The circular transmitting coils described in the previous section for the purpose of field analysis are usually used in conventional transcutaneous transformers [4], [8], [9]. However, the circular-shaped coils cannot make use of the patient's back area effectively, so they are not adopted in the prototype test and analysis. In order to better fit the transmitting coil to a vest with maximal coverage area and minimal alignment sensitivity, a rounded rectangular shape transmitting coil is proposed (see Fig. 5). It has two turns, and each turn is made of six 1.2-mm diameter copper wires connected in parallel to reduce the conduction loss. A clearance of 0.8 mm between loops is introduced to reduce the proximity effect at high frequency (a few MHz). The coil is divided into eight segments to significantly reduce the required operating voltage and dielectric loss [13], [14].

A. Field Pattern

The *H*-field of the proposed transmitting coil was simulated using FEA. The simulated result was verified in measurement. A custom-made sensing coil with a diameter of 10.3 mm was used to measure H_z. The excitation current for both simulation and measurement was set to 1 A. In the FEA model, each turn of the coil comprising six circular wires that were connected in parallel, was simulated by a single conducting wire with a rectangular cross section of $5.2\,\text{mm} \times 2.4\,\text{mm}$. This significantly reduced the number of mesh elements, and thus the computation time and the required computer memory. Fig. 6(a) shows the simulated and measured H_z along the z-axis. On the z-axis, at $z = 10$ cm, H_z drops to about 50% of the value at $z = 0$ cm, and the rate of change of H_z is –1.1%/mm. Fig. 6(b) and (c) shows H_z along the x- and y-directions, respectively, at $z = 10.7$ cm. The measured results agree well with the simulation. The field is plotted within a range of ± 7 cm to demonstrate that the proposed rounded rectangular transmitting can still provide uniform magnetic field even in an extreme situation of misalignment of ± 5 cm. Since the transmitting coil length in the y-direction is longer than in the x-direction, the variation of H_z along the x-direction (8.82%) is larger than that along the y-direction (3.65%) within the range of ± 5 cm.

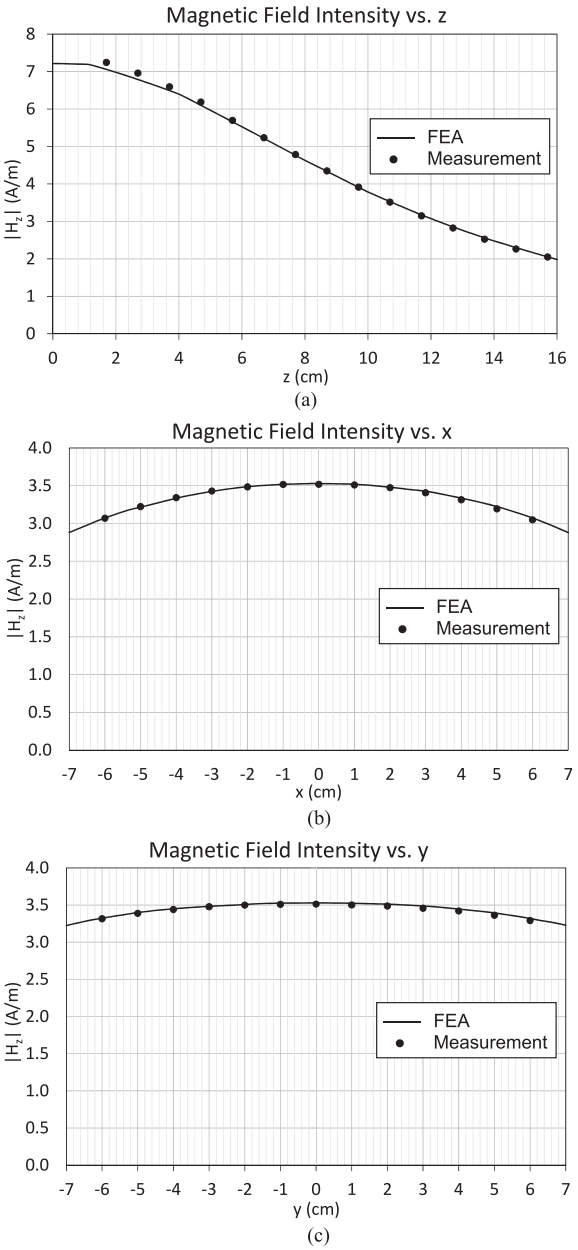

Fig. 6. Simulated and measured H_z along the (a) z-axis, (b) x-axis at $z = 10.7$ cm, and (c) y-axis at $z = 10.7$ cm of the proposed transmitting coil.

B. Electrical Characteristics

Fig. 7 shows the inductance and winding resistance of the proposed transmitting coil measured with an HP4194A impedance analyzer. We found that the parasitic intrawinding capacitance between turns causes a self-resonance around 20 MHz, so the measurement accuracy at several MHz is significantly affected. Since the coil does not include nonlinear ferrite material, its inductance $(2.72\,\mu\text{H})$ should not change substantially with frequency and can be obtained in the flat region around 1 MHz. In contrast, the winding resistance at several MHz cannot be obtained from this measurement because it is frequency-dependent due to the skin effect. The winding resistance at the operating frequency of several MHz will be obtained in the next section

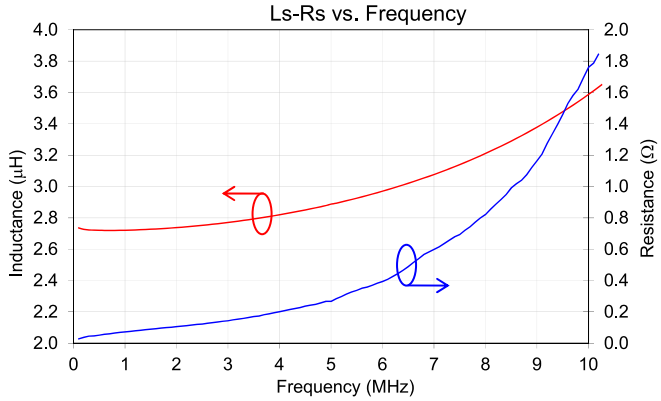

Fig. 7. Measured inductance and resistance of the proposed transmitting coil.

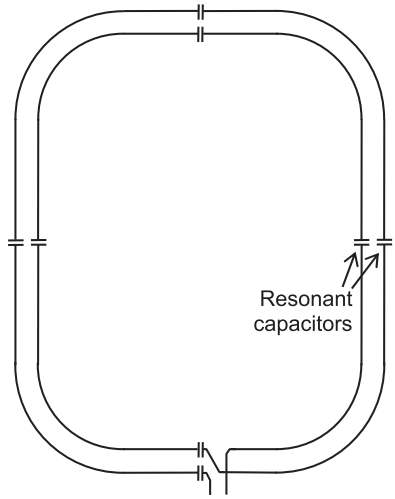

Fig. 8. Circuit schematic for the segmented proposed coil.

using a novel coil segmentation technique that eliminates the self-resonance effect as was illustrated in earlier work [14].

C. Coil Segmentation

The energy transfer system is designed to operate at the 6.78 MHz industrial, scientific and medical (ISM) band. The coil input impedance at the no-load condition is $2\pi f L_t = 2\pi(6.78\,\text{MHz})(2.72\,\mu\text{H}) = 116\,\Omega$ when the winding resistance is negligible. By using Ohm's Law, when the excitation current $I_t = 1\,\text{A}_{\text{rms}}$, an excitation voltage of $116 V_{\text{rms}}$ would be required to overcome the back electromotive force (emf) of the transmitting coil self-inductance. In higher power applications, such as powering a heart-pump (e.g., $I_t = 5\,\text{A}_{\text{rms}}$), the required voltage will be proportionally increased to $579\,\text{V}_{\text{rms}}$ (or 819V_{pk}). Such a high voltage requirement over the transmitting coil is obviously a major concern in terms of patient safety and manufacturing cost.

Recently, we demonstrated that dividing an energy coupling coil into multiple segments using resonant capacitors can significantly reduce the coil voltage to a safe level [13]–[15]. Here, we apply this technique to reduce the required voltage for the proposed coil. Fig. 8 shows a circuit schematic of the coil di-

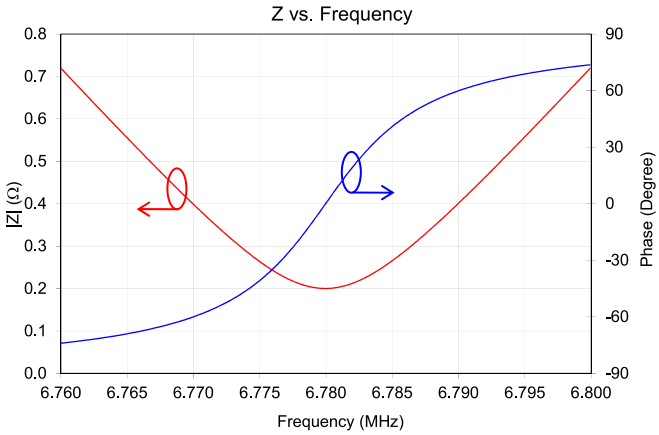

Fig. 9. Measured impedance magnitude and phase of the segmented transmitting coil tuned to 6.78 MHz.

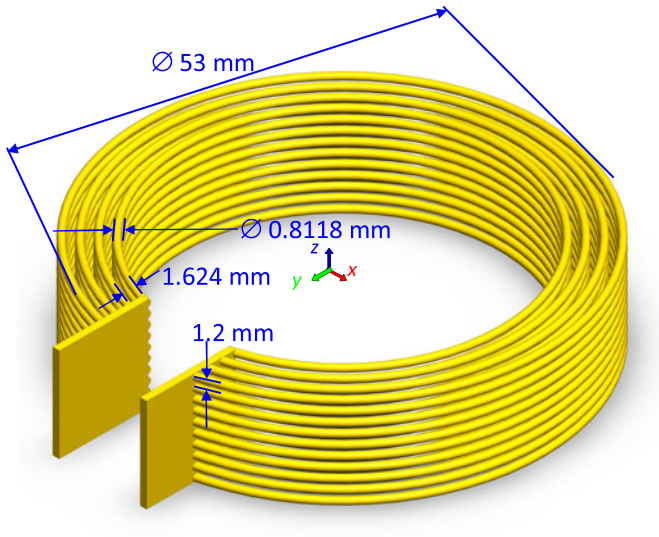

Fig. 10. A 3-D drawing of the energy receiving coil.

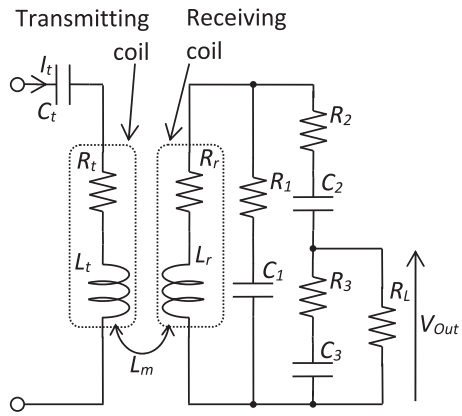

Fig. 11. Equivalent circuit model of the coupling circuit.

vided into eight segments. The voltage across each segment approximately equals the required voltage for the unsegmented coil divided by the number of segments, which is $72\,\mathrm{V_{rms}}$ in the eight-segment configuration when $I_t = 5\,\mathrm{A_{rms}}$. The segment voltage can be further reduced by increasing the number of segments. To tune the coil to the 6.78 MHz ISM band, the required capacitance for each resonant capacitor is 1.623 nF. The impedance of the segmented coil was measured and is shown in Fig. 9. At the resonant frequency, the induced voltage across each coil segment is almost canceled by the adjacent capacitor voltage. Thus, the coil impedance could be minimized to $0.2\,\Omega$, which is mainly caused by the winding resistance, instead of the coil inductance. As a result, with the coil segmentation technique the high-voltage requirement for overcoming the coil's high reactance can be eliminated and the transmitter voltage can be significantly reduced.

IV. Energy Coupling Analysis

A. Energy Receiving Coil and Resonance Circuit

The receiving coil used in the energy coupling system is shown in Fig. 10. The coil has a diameter of 5.3 cm and a height of 1.24 cm. It has only one turn but comprises four layers of ten 20 AWG copper wires connected in parallel. The separation between two layers of wires is 1.624 mm and that between two wires on the same layer is 1.2 mm.

The receiving coil was tuned to 6.78 MHz with a capacitor network shown in Fig. 11. While all the capacitors $C_1 - C_3$ are used to set the resonant frequency, C_2 and C_3 form a low-loss reactive potential divider to set the output voltage to the desired level [12]. The equivalent-series-resistance (ESR) of capacitors C_1, C_2, and C_3 are represented by R_1, R_2, and R_3, respectively. The self-inductance and winding resistance of the transmitting and receiving coils are represented by L_t, R_t, L_r, and R_r, respectively. The capacitor C_t represents the resultant series capacitance of the resonant capacitors used to segment the transmitting coil. The mutual inductance between the transmitting and receiving coils is denoted by L_m.

As shown in Fig. 10, since the coil conduction path is short and radially thick, the measured receiving coil resistance and inductance are very sensitive to the locations of the coil terminals connected to the impedance analyzer. This issue can be eliminated by using the method illustrated in the Appendix where the coil resistance and inductance are derived in the actual operating configuration with the resonant capacitors attached.

The frequency response of the energy coupling coils was measured. The receiving coil was tuned to 6.78 MHz with $C_1 = 11.889$ nF and $C_2 = C_3 = 2$ nF, and placed parallel and coaxial to the transmitting coil with a separation of 7.7 cm. Fig. 12 shows the output voltage normalized to the transmitting coil current versus frequency under no-load and $50.5\,\Omega$ load conditions. The 3-dB bandwidths of the unloaded and loaded coil were 22 and 78 kHz, respectively. The increased bandwidth at loaded condition indicates that precise fine-tuning of the receiving coil may not be necessary if the coil is sufficiently loaded.

B. Circuit Analysis

The circuit model shown in Fig. 11 was developed to predict the power losses and output power with a given transmitting current I_t, and therefore the energy efficiency. By using loop

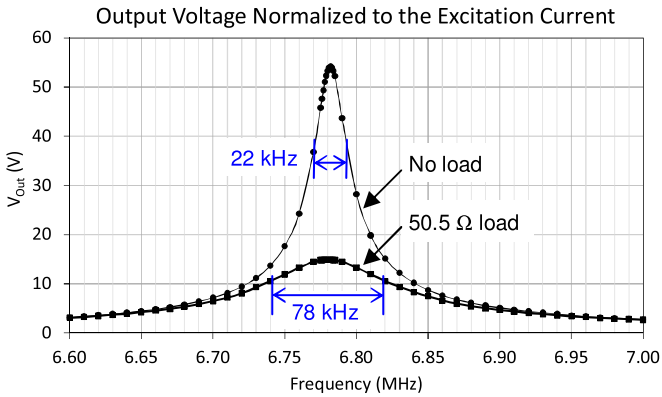

Fig. 12. Measured receiver output voltage normalized to the transmitting coil excitation current versus frequency under no-load and 50.5W load conditions when $x = y = 0$.

analysis, the load power is given by

$$P_L = \frac{\omega^2 L_m^2 |I_t|^2}{\left| Z_r \left(Z_{C2} \frac{R_L + Z_{C3}}{R_L Z_{C3} Z_{C1}} + \frac{1}{Z_{C1}} + \frac{R_L + Z_{C3}}{R_L Z_{C3}} \right) + Z_{C2} \frac{R_L + Z_{C3}}{R_L Z_{C3}} + 1 \right|^2 R_L} \tag{2}$$

where $\omega = 2\pi f$, f is the operating frequency, $Z_r = R_r + j\omega L_r$, $Z_{C1} = R_1 + \frac{1}{j\omega C_1}$, $Z_{C2} = R_2 + \frac{1}{j\omega C_2}$, and $Z_{C3} = R_3 + \frac{1}{j\omega C_3}$.

The power losses of the transmitting and receiving coils are, respectively, given by

$$P_t = |I_t|^2 R_t \tag{3}$$

$$P_r = \frac{\omega^2 L_m^2 \left| Z_{C2} \frac{R_L + Z_{C3}}{R_L Z_{C3} Z_{C1}} + \frac{1}{Z_{C1}} + \frac{R_L + Z_{C3}}{R_L Z_{C3}} \right|^2 |I_t|^2 R_r}{\left| Z_r \left(Z_{C2} \frac{R_L + Z_{C3}}{R_L Z_{C3} Z_{C1}} + \frac{1}{Z_{C1}} + \frac{R_L + Z_{C3}}{R_L Z_{C3}} \right) + Z_{C2} \frac{R_L + Z_{C3}}{R_L Z_{C3}} + 1 \right|^2}. \tag{4}$$

The power efficiency of the energy coupling circuit is given by

$$\eta = \frac{P_L}{P_L + P_t + P_r}. \tag{5}$$

C. Mutual Inductance Measurement

To predict the output power and energy efficiency using the formulas derived in the previous section, the mutual inductance between the energy coupling coils was measured. In this measurement, the transmitting coil current was set to 1 A_{rms}. The mutual inductance values were measured when the energy receiving coil was located at different positions along the $x-$, $y-$, and z-directions. Fig. 13 shows the mutual inductance varied with displacement of the receiving coil along the z-axis. Figs. 14 and 15 show the mutual inductance when the receiving coil displaced along the x- and y- directions, respectively, at $z = 7.7$ and 10.7 cm. Similar to the H-field distribution of the proposed transmitting coil presented in Section III-A, the mutual inductance variation in the x-direction is larger than that in the y-direction. Within the range of ± 5 cm, at $z = 7.7$ cm, the mutual inductance variations in the x- and y- directions were 7.4% and 3.2%, respectively; at $z = 10.7$ cm, the variations were 10% and 5.8%, respectively.

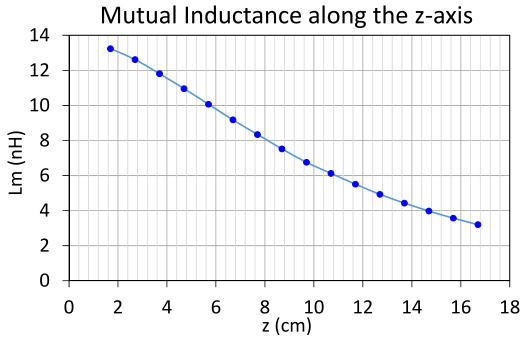

Fig. 13. Measured mutual inductance between the transmitting and receiving coils along the z-axis.

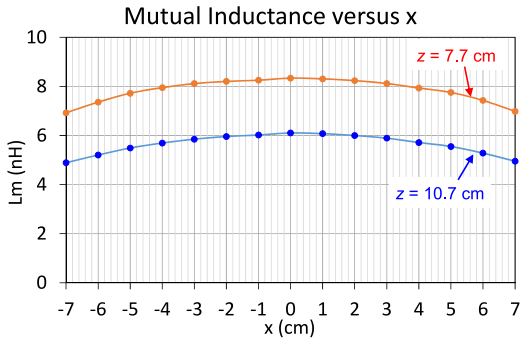

Fig. 14. Measured mutual inductance between the transmitting and receiving coils versus x when $y = 0$.

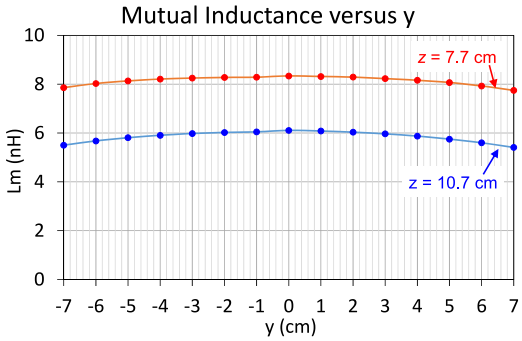

Fig. 15. Measured mutual inductance between the transmitting and receiving coils versus y when $x = 0$.

D. Output Power and Energy Efficiency

The output power and efficiency of the energy coupling coils with different load conditions were calculated based on (2)–(5) and verified by experimental measurement. Fig. 16 shows the measured and calculated output power and efficiency when the

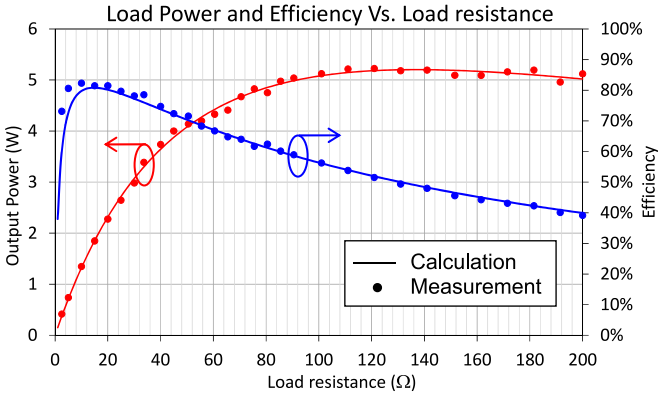

Fig. 16. Calculated and measured output power and efficiency versus load resistance at $x = y = 0$, $z = 7.7$ cm and $I_{\rm t} = 1\ {\rm A_{rms}}$.

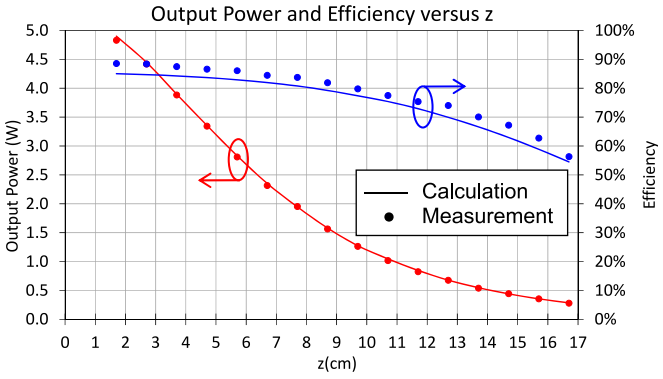

Fig. 17. Calculated and measured output power and efficiency along the z-axis when $I_{\rm t} = 1\ {\rm A_{rms}}$ and $R_{\rm L} = 16\Omega$.

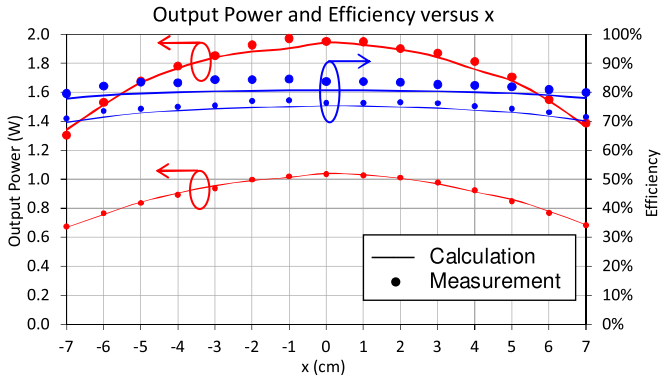

Fig. 18. Calculated and measured output power and efficiency versus x when $y = 0$, $z = 7.7$ cm (thick lines) and 10.7 cm (thin lines), and $I_{\rm t} = 1\ {\rm A_{rms}}$ and $R_{\rm L} = 16\,\Omega$.

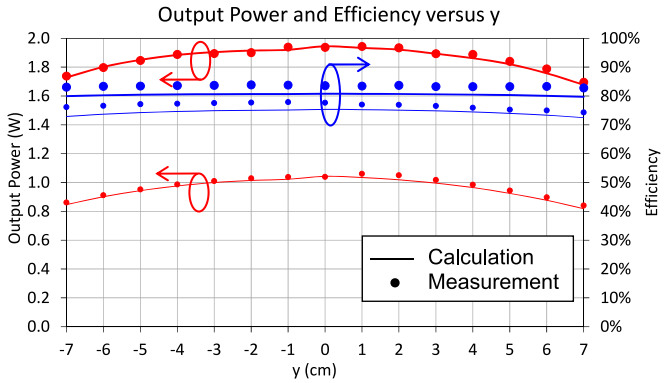

Fig. 19. Calculated and measured output power and efficiency versus y when $x = 0$, $z = 7.7$ cm (thick lines) and 10.7 cm (thin lines), and $I_{\rm t} = 1\ {\rm A_{rms}}$ and $R_{\rm L} = 16\,\Omega$.

receiving coil was placed in parallel and coaxial to the transmitting coil with a separation $z = 7.7$ cm. The transmitting coil current was set to 1 $\rm A_{rms}$ and the load resistance R_L ranged from 2.5 to 200 Ω. In the system prototype, low-loss radio-frequency capacitors were used for $C_1 - C_3$, so the capacitors' ESRs $R_1 - R_3$ were much lower than the receiving coil winding resistance and could be ignored. From Fig. 16, maximum energy transfer occurred at a load resistance of about 130 Ω, but the energy efficiency dropped to about 50%. In high-power implant applications, operating the energy transfer system around the maximum energy efficiency region is preferred to minimize the power dissipation and extend the external battery life. Maximum energy efficiency of more than 80% could be achieved while having a load resistance between 11 and 20 Ω. In this load region, the output power increases with load resistance, and equals to 2.3 W with a load of 20 Ω. The measured and calculated maximum efficiency were 82.3% and 80.8%, respectively.

The output power and efficiency were also calculated and measured in different locations along the $x-$, $y-$, and z-directions with an excitation of 1 $\rm A_{rms}$ and a load resistance of 16 Ω. Fig. 17 shows the output power and efficiency along the z-axis, which decreased with the coil separation z. The output power and efficiency were 1.95 W and 80.8% at $z = 7.7$ cm, respectively. These values dropped to 1.0 W and 75% at $z = 10.7$ cm. The output power variations at $z = 7.7$ and 10.7 cm were –1.6 and–1.7%/mm, respectively, while the efficiency variations at both locations were less than 1%/mm.

Figs. 18 and 19 show the calculated and measured output power and efficiency along the x- and y-directions, respectively, when $z = 7.7$ and 10 cm. Variations in the output power and efficiency along the x-direction were greater than that in the y-direction. These characteristics were predicted by the above-mentioned H-Field and mutual inductance profiles. In a conventional transcutaneous transformer, the maximum allowable lateral misalignment has to be around 1 cm to achieve a reasonable power efficiency. With our proposed design, the output power and efficiency variation was less than 2.7% and 0.4%, respectively, in these limits. In a more extreme situation where the misalignment was increased to ±5 cm, the output power variations in x- and y-directions were 14.2% and 5%, respectively, at $z = 7.7$ cm. When $z = 10.7$ cm, the output power variations in the x- and y-directions were 19.1% and 9.1%, respectively, and the efficiency variations in both of the directions and coil separations were less than 3.3%. It should be noted that the transferred power variations could be compensated by using a dedicated control scheme that adjusted the transmitting coil current, but it failed to improve the energy efficiency variation. Since the coupling coils efficiency did not vary significantly, even in the

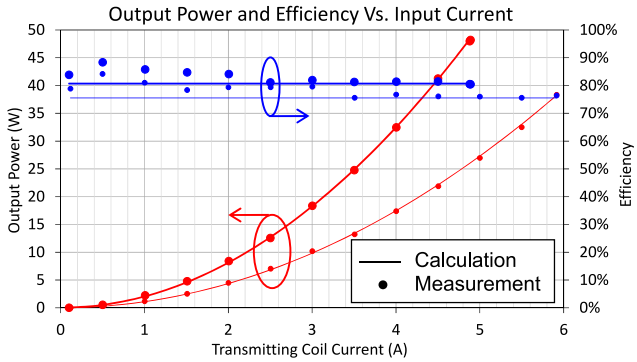

Fig. 20. Calculated and measured output power and efficiency versus transmitting coil current when $x = y = 0$, z = 7.7 cm (thick lines) and 10.7 cm (thin lines), and $R_{\rm L} = 16.8\ \Omega$.

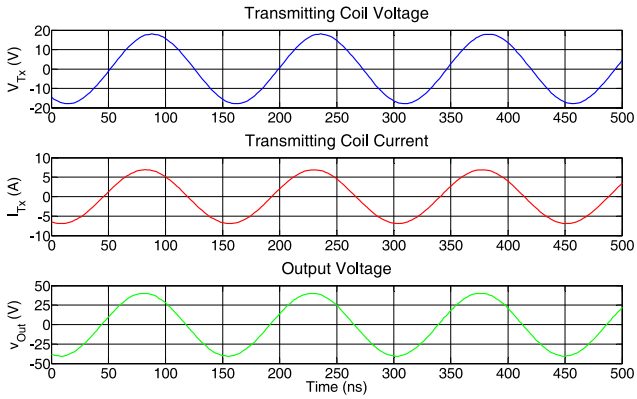

Fig. 21. Measured waveforms of the transmitting coil voltage, $V_{\rm Tx}$, current $I_{\rm Tx}$, and output voltage, $V_{\rm Out}$ when $P_{\rm out} = 48.2$ W when the receiving coil is located at $x = y = 0$, and $z = 7.7$ cm.

extreme situation of misalignment of ± 5 cm, the transmitting coil with an appropriate current control can, in principle, wirelessly transfer power with stable output power and efficiency.

The output power and efficiency were calculated and measured with different excitation current levels (see Fig. 20). The load resistance was set to $16.8\,\Omega$. As predicted by (2), the output power was proportional to the square of the transmitting coil current. This equation also predicts that if mutual inductance declines, the required excitation current should be simultaneously increased to achieve the same output power. The decrease of mutual inductance is primarily caused by the increase of coil separation (see Figs. 13–15). At $z = 7.7$ cm, the maximum output power was 48.2 W when I_t was 4.89 $\rm A_{rms}$. The measured transmitting coil voltage, current, and output voltage waveforms are shown in Fig. 21. From the measured input voltage waveform, the coil excitation only reached $12.6\,\rm V_{rms}$, which is much less that that required for the conventional unsegmented transmitting coils described in Section III-C. At increasing distances in z up to 10.7 cm, we observed a maximum output power of 38.3 W for a current $I_t = 5.92\,\rm A_{rms}$. We could not investigate higher power levels, since we reached the maximum output power capability of the RF power amplifier adopted for driving the transmitting coil.

V. Verification With a Circulatory Model

The operation of the mid-range wireless energy coupling coils was verified with a simplified circulatory model driven by a 24-V dc pump as shown in Fig. 22. The dc pump, which was used to represent an LVAD actuator, propelled the water flow cycling throughout the circulatory model. This is a simulated model made of plastic tubes and a heart-shaped water reservoir. Energy coupling capability with a coil separation of 10 cm was tested. The receiving coil was placed next to the pump. The dc pump (DC40F-2460, BLDC Pump Technology, Shenzhen China) was powered by the proposed wireless energy coupling method illustrated by the circuit schematic in Fig. 23. An additional load R_L with a resistance of $152\,\Omega$ was connected in parallel to the dc pump to represent the power consumption of auxiliary circuits, such as motor drive, control, and communication. The measured load power was 19.7 W, and the transmitting voltage and current were $8.57\,\rm V_{rms}$ and $4.23\,\rm A_{rms}$, respectively. Although the power efficiency of the energy coupling coils was about 75%, the whole efficiency including the diode rectifier is reduced to 54%. In this demonstration, a conventional full-bridge diode is adopted to convert the received ac voltage to dc. The power loss of the rectifier could have been further reduced by using synchronous rectifier. By adjusting the transmitting coil current, the output voltage was set to 24 V. The transmitting coil voltage and current waveforms were captured (see Fig. 24). These results verify that, even in high-power applications, the high excitation voltage necessary for overcoming the back emf induced by a larger transmitting coil is not necessary with the segmented coils developed in this study.

VI. Discussions

A. Specific Energy Absorption Rate (SAR) Evaluation

Patient's safety is one of the most important factors in the design of medical devices. We demonstrated that using the coil segmentation technique, the required transmitting coil excitation voltage can be significantly reduced to a safe level (e.g., around 10 V) while conventional unsegmented transmitting coils require up to several kV. Although the coil voltage and thus the electric field can be minimized, the high-frequency alternating magnetic field generated by the transmitter will induce eddy current in conductive body tissues and increase the body temperature.

In order to evaluate the magnetic energy absorption in the patient's body, a three dimensional (3-D) FEA human thorax model simulating the tissue conductivity was developed. The FEA model is similar to that used in [32] for the abdomen, but the small intestine is replaced by lung tissue and a layer of bone is added to simulate the rib cage. The thorax model is in cylindrical shape with a diameter of 300 mm and a height of 400 mm as shown in Fig. 25. The thicknesses of skin, fat, muscle, and rib bone are 5, 10, 15, and 8 mm, respectively. The diameters of the spine and blood vessels representing the aorta and vena cava are 30 and 20 mm, respectively. The tissue conductivity (see Table II) at 6.78 MHz were obtained based on the 4-Cole–Cole model described in [33] using the RF_Tools MATLAB program developed by the Center for NMR Research at the Penn State University [34].

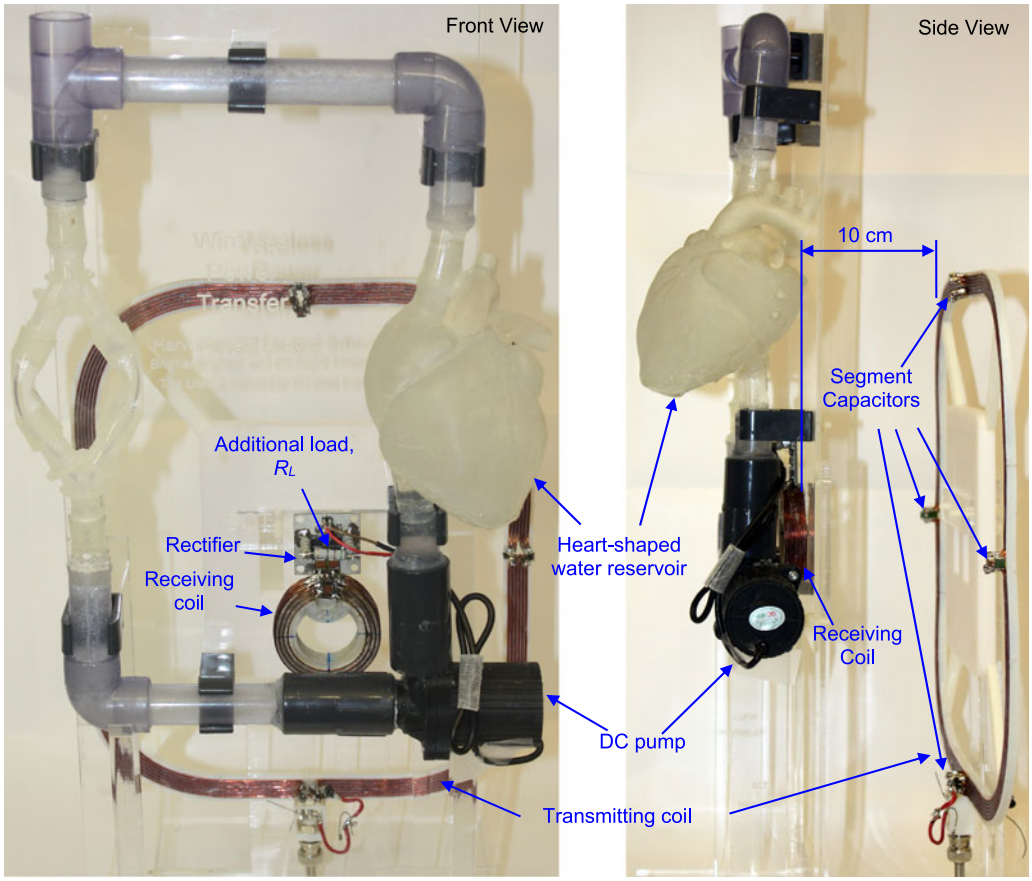

Fig. 22. Front and side views of the wirelessly powered circulatory model.

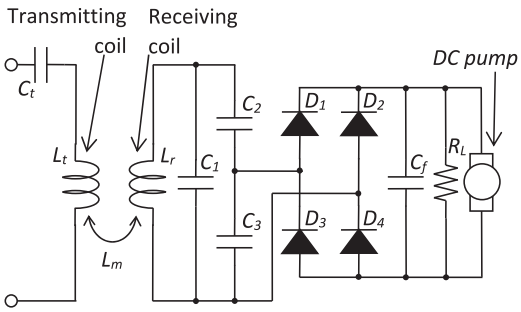

Fig. 23. Energy coupling circuit for the circulatory model.

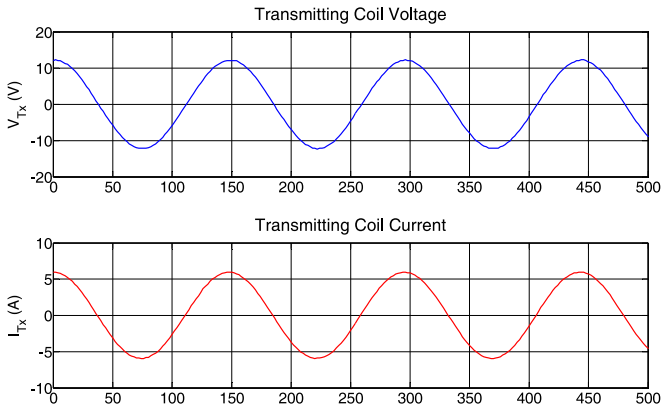

Fig. 24. Measured waveforms of the transmitting coil voltage, V_{Tx}, and current I_{Tx}, when the receiver is loaded with a 24-V dc pump and a parallel 152-Ω resistor.

From the FEA program, power absorption densities of body tissues were obtained. However, in the safety evaluation of magnetic field exposure, SAR instead of power absorption density should be evaluated [35]. The SAR, which is defined as the power absorption per kilogram of body tissue, can be deduced by

$$\text{SAR (W/kg)} = \frac{\text{Power absorption density (W/m}^3\text{)}}{\text{Mass density (kg/m}^3\text{)}} \quad (6)$$

where the mass density of the tissues are listed in Table II.

According to the guidelines from the International Commission on Non-Ionizing Radiation Protection (ICNIRP) [35], the localized SAR of 10 g contiguous tissue should be lower than 2 W kg^{-1} for general public exposure and 10 W kg^{-1} for occupational exposure when the frequency ranges from 100 kHz to 10 MHz to avoid tissue damage. We choose the more stringent restriction (2 W kg^{-1}) for the sake of safety as the patient using the heart pump would be exposed to the magnetic field continuously. From the simulated results, it is found that the peak SAR occurred at the region close to the transmitting coil.

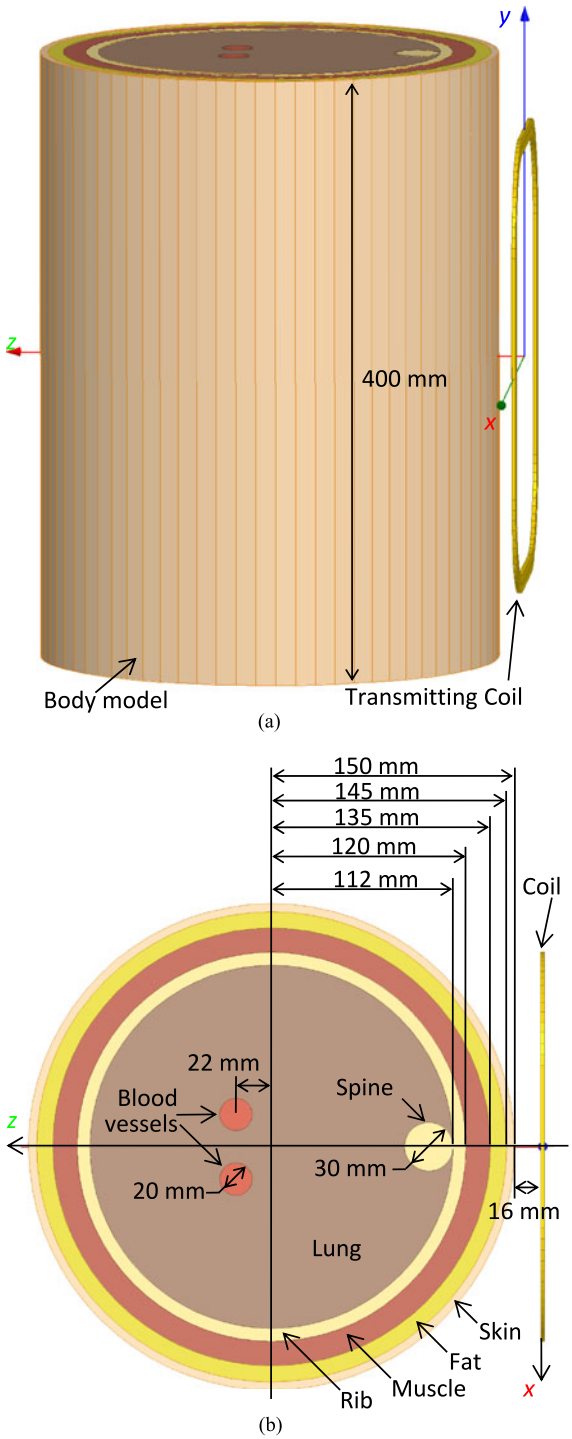

Fig. 25. (a) Three-dimensional view and (b) top-view of a FEA simulation model for the evaluation of SAR in human tissues when the proposed coil is used.

TABLE II
CONDUCTIVITY AND MASS DENSITY OF BODY TISSUES.

Tissue	Conductivity (S m^{-1})	Mass density (kg m^{-3})
Blood	1.0673	1060 [37]
Bone	0.11585	1330 [38]
Fat	0.027776	960 [38]
Lung	0.21036	246 [36]
Muscle	0.6021	1065 [38]
Skin	0.14692	1090 [39]

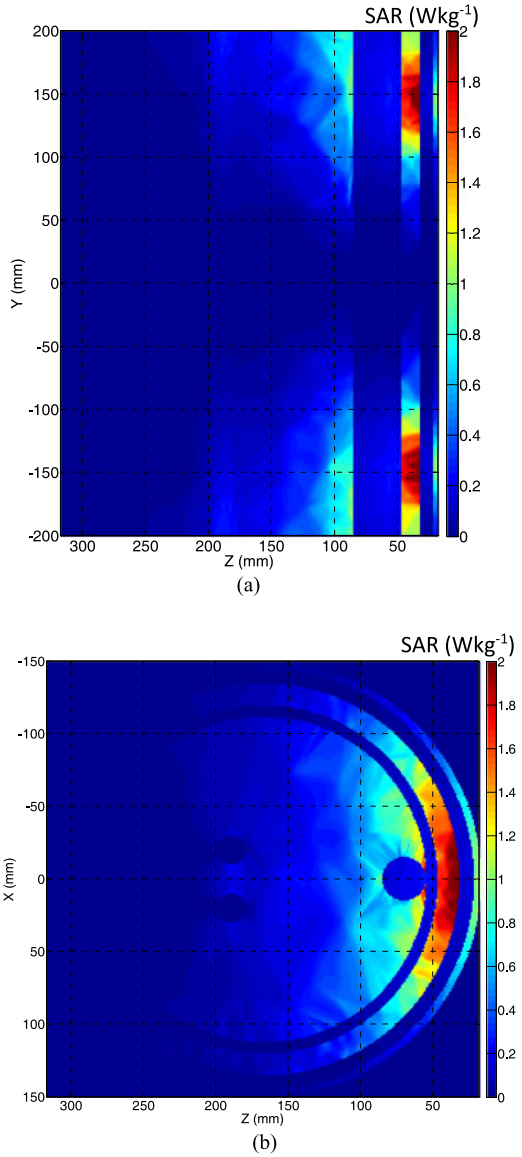

Fig. 26. Simulated SAR of the body model on the (a) y–z plane at $x = 0$ and (b) x–z plane at $y = 145$ mm when the transmitting coil current is 4.89 A_{rms}.

Fig. 26 shows the simulated SAR on the $y - z$ plane at $x = 0$ and $x - z$ plane at $y = 145$ mm where peak SAR occurs. In this simulation, the transmitting coil current is $4.89\,A_{rms}$, which represents the excitation for achieving an output power of 48 W demonstrated in Section IV-D. We found that the maximum localized SAR was lower than the suggested restriction of 2 W kg^{-1} when the separation between the coil and skin is more than 15 mm. Unlike conventional transcutaneous transformers, which have to be placed against the skin, larger transmitting coils can be placed a little farther away from the skin to reduce the localized SAR. Thus, the coil-skin separation was set to 16 mm

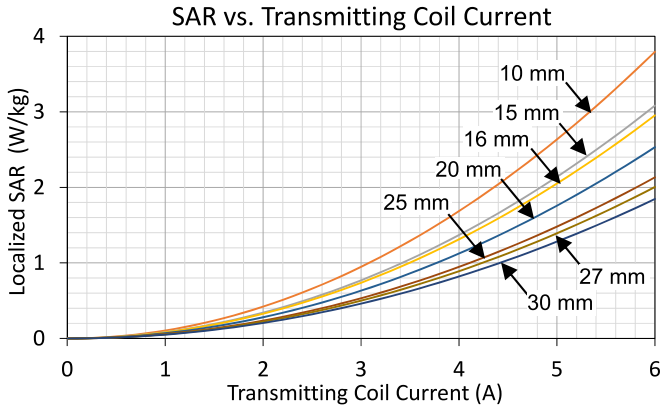

Fig. 27. Simulated maximum localized SAR of 10 g contiguous tissue of the body model versus transmitting coil current with different coil-skin separation from 10 to 30 mm.

in the simulation setup but could be further increased to provide a larger safety margin. To estimate the required coil-skin separation, we have performed a series of simulations to determine the maximum localized SAR of 10 g contiguous tissue with different transmitting coil currents and coil-skin separations from 10 to 30 mm as shown in Fig. 27. The result shows that the localized SAR is proportional to the transmitter current, but decreases with the coil-skin separations. Thus, it is suggested that the coil-skin separation should be increased for larger transmitting coil current to comply with the ICNIRP guidelines. In the case of the dc pump powering system described in the previous section, the transmitting current was $4.23\,\mathrm{A_{rms}}$, the minimum coil-skin separation is about 10 mm. Based on the FEA results, when the coil-skin separation is large enough, the proposed segmented coil transmitter could in principle be safely used to transfer energy to implantable devices with relatively high power consumption, such as heart pump.

B. Experimental Temperature Measurement

The temperature rise caused by magnetic energy absorption of tissues was estimated using a solution simulating the conductivity of human muscle. The solution was made of sodium chloride with a conductivity of 0.62 S m^{-1} at 6.78 MHz. The solution was filled in a rectangular container with dimensions of 30 cm (W) $\times$ 20 cm (D) $\times$ 49 cm (H). The separation between the transmitting coil and the solution was 16 mm. Fiber optic temperature sensors were used to measure the solution, receiving coil case, and ambient temperatures. The sensor for measuring the solution temperature was placed close to the transmitting coil in where the maximum SAR occurred, while that for measuring the ambient temperature was placed on the container. A plastic case for the receiving coil was fabricated. The wall thickness of the case is 2 mm. In the temperature measurement, the receiving coil was submerged in the solution, sealed with a plastic bag with a thickness of $50\,\mu\mathrm{m}$, and loaded with the $16.8\,\Omega$ resistor that used in Section IV-D. The separation between the transmitting and receiving coils is 10 cm. The temperature sensor was placed on the plastic bag and close to the coil winding where maximum temperature occurred. The temperature measurement sampling rate was 1 sample/s and the duration was 1 h. Throughout the measurement, the solution was still in the container without forced cooling and was thermally isolated from the transmitting coil to minimize the heat transfer by thermal conduction and convection from the coil. The measurement was performed in room temperature kept between 22 °C and 23 °C.

According to the ICNIRP guidelines, temperature rises of more than 1 °C–2 °C can have adverse health effects, so we evaluated the maximum excitation current that would increase the temperature by less than 1 °C. In the experimental setup, when the transmitting coil was excited by $4.8\,\mathrm{A_{rms}}$, the temperature rises of the solution and receiving coil case after 1 h were 0.9 °C and 0.8 °C, respectively. Compared to the actual human body, the temperature rises evaluated by this experimental setup were overestimated because first, the fluid in the container was still, but in the human body, blood flow and perfusion, air exchange in the lung, and sweating would act as a forced cooling to effectively carry away the heat from the receiving coil and magnetic energy absorption in tissues. Second, the conductivity of the solution simulating the muscle tissue, which is the highest among the solid tissues in the thorax, was used in the experiment. Also, a substantial volume of the lung is filled with air, which is not electrically conductive and so does not absorb magnetic energy. Thus, the magnetic energy absorption in the solution was higher than that in the actual human tissues in the thorax. Third, there is heat loss from the body to air by thermal conduction and convection since the body temperature (37 °C) is usually higher than the ambient temperature. However, since the experiment was conducted in room temperature and the temperature increase of the solution is less than 1 °C, there is no obvious heat transfer from the solution to the air. As a result, in principle, the actual temperature rise of body tissue caused by the wireless transfer system should be lower than that estimated by the experiment, and so the allowable excitation current should be higher than $4.8\,\mathrm{A_{rms}}$. Although this excitation level is already sufficient to power a dc pump as demonstrated in Section V, a more sophisticated human body thermal model or *in vivo* animal experiment could be adopted to determine the highest allowable excitation current and power transfer rate without exceeding the ICNIRP limit.

VII. Conclusion

In this extended work, apart from just a specific application of our previously proposed segmented coil transmitter, more importantly, we demonstrated its high power transfer capability with a safe transmitter voltage of around $10\,\mathrm{V_{rms}}$. This capability has not been reported in the literature on intermediate-range wireless power transfer. We believe that the finding and analysis presented in this paper would have significant values in both power electronics and the industry of live-saving medical implantable devices. These results demonstrate that wireless power transfer using a segmented coil can drive relatively high power applications, such as heart pumps, while maintaining a safe voltage. Based on the magnetic field analysis of transmitting coils with different dimensions, we determined that transmitting coils with larger inner and outer diameters can provide both a wider

transmission range and lower alignment sensitivity. We developed a $24 \times 30\ \mathrm{cm}^2$ transmitting coil in a rounded rectangular shape. Its energy transfer capability was tested with a 5.3 cm, single turn receiving coil at different coil separations. The measured output power and efficiency with a coil separation of 7.7 cm were higher than 48 W and 80%, respectively. When the coil separation was increased to 10.7 cm, the output power and efficiency were 38 W and 75%, respectively. Experimental validation has also been carried out in LVAD model. The energy coupling coils were evaluated with a 24 V DC pump, which was used to propel fluid through a circulatory model. This pump was driven in parallel to an additional load of $152\ \Omega$, representing the power consumption of auxiliary circuits of the implanted pump. Even with a coil separation of 10 cm, the measured load power was 19.7 W, and the required transmitting coil voltage was only $8.57\ \mathrm{V_{rms}}$. The experimental results verified our hypothesis that the coil segmentation technique can achieve mid-range wireless power transfer without requiring high-voltage excitation.

APPENDIX
METHOD FOR DERIVING THE RECEIVING COIL RESISTANCE AND INDUCTANCE

Let Z_{Cr} be the resultant impedance of the resonant capacitor network in the receiving circuit shown in Fig. A.1

$$Z_{Cr} = \frac{Z_{C1}\left(Z_{C2} + Z_{C3}\right)}{Z_{C1} + Z_{C2} + Z_{C3}} \tag{A.1}$$

where $Z_{C1} = R_1 + \frac{1}{j\omega C_1}, Z_{C2} = R_2 + \frac{1}{j\omega C_2}$, and $Z_{C3} = R_3 + \frac{1}{j\omega C_3}$.

By using the potential divider formula twice, the output voltage V_{Out} at no-load condition is given by

$$V_{\mathrm{Out}} = \frac{Z_{C3}}{Z_{C2} + Z_{C3}} \frac{Z_{Cr}}{j\omega L_r + R_r + Z_{Cr}} j\omega L_m I_t. \tag{A.2}$$

Since we use low-ESR capacitors in the receiving resonance circuit $R_i << 1/\omega C_i$, where $i = 1$ to 3, (A.1) becomes

$$Z_{Cr} = \frac{C_2 + C_3}{j\omega\left(C_1C_2 + C_1C_3 + C_2C_3\right)}. \tag{A.3}$$

At the resonant frequency

$$j\omega L_r + Z_{Cr} = 0. \tag{A.4}$$

Substituting (A.3) and (A.4) into (A.2)

$$V_{\mathrm{Out}} = \frac{C_2}{C_2 + C_3} \frac{C_2 + C_3}{j\omega\left(C_1C_2 + C_1C_3 + C_2C_3\right) R_r} j\omega L_m I_t$$

$$\Rightarrow R_r = \frac{L_m I_t}{\left(\frac{C_1 C_3}{C_2} + C_1 + C_3\right) V_{\mathrm{Out}}}. \tag{A.5}$$

From Figs. 13 and 12, at $z = 7.7\,\mathrm{cm}$, $L_m = 8.345\,\mathrm{nH}$, and V_{Out} normalized to the transmitting coil excitation current is 53.344 V when $C_1 = 11.889\ \mathrm{nF}, C_2 = C_3 = 2\ \mathrm{nF}$. Substituting these parameters into (A.5), the receiving coil resistance is obtained as $6.069\ \mathrm{m\Omega}$. From (A.3) and (A.4), the inductance is obtained as 42.75 nH.

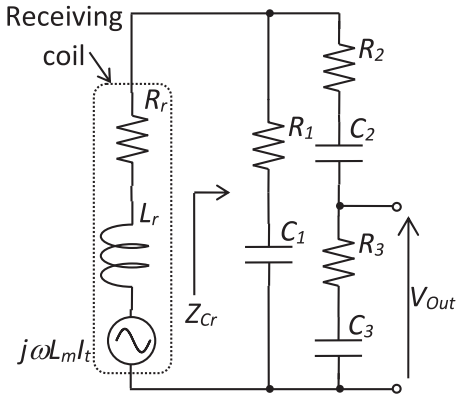

Fig. A.1. Receiving circuit.

REFERENCES

[1] H. Miura, S. Arai, F. Sato, H. Matsuki, and T. Sato, "A synchronous rectification using a digital PLL technique for contactless power supplies," *IEEE Trans. Magn.*, vol. 41, no. 10, pp. 3997–3999, Oct. 2005.

[2] A. Ghahary and B. H. Cho, "Design of transcutaneous energy transmission system using a series resonant converter," *IEEE Trans. Power Electron.*, vol. 7, no. 2, pp. 261–269, Apr. 1992.

[3] J. W. Fuller, "Apparatus for efficient power transfer through a tissue barrier," *IEEE Trans. Biomed. Eng.*, vol. BME-15, no. 1, pp. 63–65, Jan. 1968.

[4] T. D. Dissanayake *et al.*, "A novel low temperature transcutaneous energy transfer system suitable for high power implantable medical devices performance and validation in sheep," *Artif. Organs*, vol. 34, no. 5, pp. E160–E167, May 2010.

[5] Q. Chen, S. C. Wong, C. K. Tse, and X. Ruan, "Analysis, design, and control of a transcutaneous power regulator for artificial hearts," *IEEE Trans. Biomed. Circuits Syst.*, vol. 3, no. 1, pp. 23–31, Feb. 2009.

[6] G. B. Joung and B. H. Cho, "An energy transmission system for an artificial heart using leakage inductance compensation of transcutaneous transformer," *IEEE Trans. Power Electron.*, vol. 13, no. 6, pp. 1013–1022, Nov. 1998.

[7] H. Y. Leung, D. M. Budgett, D. McCormick, and A. P. Hu, "Wireless power system for implantable heart pumps based on energy injection control," in *Proc. Progress Electromagn. Res. Symp.*, Aug. 2012, pp. 445–449.

[8] H. Y. Leung, D. M. Budgett, and A. P. Hu, "Minimizing power loss in air-cored coils for tet heart pump systems," *IEEE J. Emerg. Sel. Topics Circuits Syst.*, vol. 1, no. 3, pp. 412–419, Sep. 2011.

[9] S. Arai, H. Miura, F. Sato, H. Matsuki, and T. Sato, "Examination of circuit parameters for stable high efficiency TETS for artificial hearts," *IEEE Trans. Magn.*, vol. 41, no. 10, pp. 4170–4172, Oct. 2005.

[10] R Puers, R Carta, and J. Thoné, "Wireless power and data transmission strategies for next-generation capsule endoscopes," *J. Micromech. Microeng.*, vol. 21, no. 5, 2011.

[11] W. Xin, G. Yan, and W. Wang, "Study of a wireless power transmission system for an active capsule endoscope," *Int. J. Med. Robot. Comput. Assist. Surgery*, vol. 6, no. 1, pp. 113–122, Mar. 2010.

[12] S. C. Tang, F. A. Jolesz, and G. T. Clement, "A wireless batteryless deep-seated implantable ultrasonic pulser-receiver powered by magnetic coupling," *IEEE Trans. Ultrason., Ferroelectr, Freq. Control*, vol. 58, no. 6, pp. 1211–1221, Jun. 2011.

[13] S. C. Tang, "A low-operating-voltage wireless intermediate-range scheme for energy and signal transmission by magnetic coupling for implantable devices," *IEEE J. Emerg. Sel. Topics Power Electron.*. vol. 3, no. 1, pp. 242–251, Mar. 2015.

[14] S. C. Tang and N. J. McDannold, "Power loss analysis and comparison of segmented and unsegmented energy coupling coils for wireless energy transfer," *IEEE J. Emerg. Sel. Topics Power Electron.*. vol. 3, no. 1, pp. 215–225, Mar. 2015.

[15] S. C. Tang, D. Vilkomerson, and T. Chilipka, "Magnetically-powered implantable doppler blood flow meter," in *Proc. IEEE Int. Ultrason. Symp.*, Sep. 2014, pp. 1622–1625.

[16] L. Kim, S. C. Tang, and S. S. Yoo, "Prototype modular capsule robots for capsule endoscopies," in *Proc. 13th Int. Conf. Control, Autom. Syst.*, Oct. 2013, pp. 350–354.

[17] K. Shiba, M. Nukaya, T. Tsuji, and K. Koshiji, "Analysis of current density and specific absorption rate in biological tissue surrounding transcutaneous transformer for an artificial heart," *IEEE Trans. Biomed. Eng.*, vol. 55, no. 1, pp. 205–213, Jan. 2008.

[18] J. C. Schuder, J. H. Gold, and H. E. Stephenson, "An inductively coupled RF system for the transmission of 1 kW of power through the skin," *IEEE Trans. Biomed. Eng.*, vol. BME-18, no. 4, pp. 265–273, Jul. 1971.

[19] J. C. Schuder, H. E. Stephenson, Jr., and J. F. Townsend, "High level electromagnetic energy transfer through a closed chest wall," *IRE Int. Convention Rec., Part 9*, vol. 9, pp. 119–126, 1961.

[20] A. M. Dolan, H. E. Stephenson, S. H. Malt, J. C. Schuder, and J. W. Mackenzie, "Heat and electromagnetic energy transport through biological material at levels relevant to intrathoracic artificial heart," *Trans. Amer. Soc. Artif. Internal Organs*, vol. 12, pp. 275–281, Apr. 1966.

[21] A. Thumim, G. Reed, F. Lupo, G. Myers, and L. Cortes, "High power electromagnetic energy transfer for totally implanted devices," *IEEE Trans. Magn.*, vol. M-6, no. 2, pp. 326–332, Jun. 1970.

[22] F. W. Fraim and F. N. Huffman, "Performance of a tuned ferrite core transcutaneous transformer," *IEEE Trans. Biomed. Eng.*, vol. BME-18, no. 5, pp. 352–359, Sep. 1971.

[23] J. R. Woodbury, "Design of imperfectly coupled power transformers for dc to dc conversion," *IEEE Trans. Ind. Electr. Control Instrum.*, vol. IECI-21, no. 3, pp. 152–159, Aug. 1974.

[24] H. Matsuki, K. Nadehara, T. Watanabe, K. Murakami, and T. Yamamoto, "High-output transmitting coil with cloth structure utilizing amorphous magnetic fiber for implanted artificial heart," *IEEE Trans. Magn.*, vol. 25, no. 5, pp. 3812–3814, Sep. 1989.

[25] D. B. Geselowtiz, Q. T. N. Hoang, and R. P. Gaumond, "The effects of metals on a transcutaneous energy transmission system," *IEEE Trans. Biomed. Eng.*, vol. 39, no. 9, pp. 928–934, Sep. 1992.

[26] H. Matsuki, Y. Yamakata, N. Chubachi, S. Nitta, and H. Hashimoto, "Transcutaneous DC-DC converter for totally implantable artificial heart using synchronous rectifier," *IEEE Trans. Magn.*, vol. 32, no. 5, pp. 5118–5120, Sep. 1996.

[27] W. Fang, W. Liu, J. Qian, H. J. Tang, and P. S. Ye, "Modeling and simulation of a transcutaneous energy transmission system used in artificial organ implants," *Artif. Organs*, vol. 33, no. 12, pp. 1069–1074, Dec. 2009.

[28] H. Y. Leung, D. McCormick, D. M. Budgett, and A. P. Hu, "Pulse density modulated control patterns for inductively powered implantable devices based on energy injection control," *IET Power Electron.*, vol. 6, no. 6, pp. 1051–1057, Jul. 2013.

[29] H. Miura, S. Arai, F. Sato, H. Matsuki, and T. Sato, "A synchronous rectification using a digital PLL technique for contactless power supplies," *IEEE Trans. Magn.*, vol. 41, no. 10, pp. 3997–3999, Oct. 2005.

[30] B. H. Waters, A. P. Sample, P. Bonde, and J. R. Smith, "Powering a ventricular assist device (VAD) with the free-range resonant electrical energy delivery (FREE-D) system," *Proc. IEEE*, vol. 100, no. 1, pp. 138–149, Jan. 2012.

[31] W. R. Smythe, *Static and Dynamic Electricity*, 2nd ed. New York, NY, USA: McGraw-Hill, 1950, pp. 270–271.

[32] K. Shiba, T. Nagato, T. Tsuji, and K. Koshiji, "Analysis of specific absorption rate and current density in an energy transmission system for a wireless capsule endoscope," in *Proc. IEEE 29th Annu. Int. Conf. Eng. Med. Biol. Soc.*, Aug. 2007, pp. 6051–6054.

[33] C. Gabriel, "Compilation of the dielectric properties of body tissues at RF and microwave frequencies," Air Force Material Command, Brooks Air Force Base, San Antonio, TX, USA, AL/OE-TR-1996-0037, 1996.

[34] (2016). [Online]. Available: http://www.pennstatehershey.org/web/nmrlab/reso-urces/software/rftools

[35] International Commission on Non-Ionizing Radiation Protection, "Guidelines for limiting exposure to time-varying electric, magnetic, and electromagnetic fields (up to 300 GHz)," *Health Phys.*, vol. 74, no. 4, pp. 494–522, 1998.

[36] S. Nebuya, G. H. Mills, P. Milnes, and B. H. Brown, "Indirect measurement of lung density and air volume from electrical impedance tomography (EIT) data," *Physiol. Meas.*, vol. 32, no. 12, pp. 1953–1967, Dec. 2011.

[37] (2016). [Online]. Available: http://physics.nist.gov/PhysRefData/XrayMassCoef/tab2.html

[38] R. Bartlett, C. Gratton, and C. G. Rolf, *Encyclopedia of International Sports Studies*, Abingdon: Routledge, 2009, p. 164.

[39] R Kramer *et al.*, "All about FAX a female adult voXel phantom for Monte Carlo calculation in radiation protection dosimetry," *Phys. Med. Biol.*, vol. 49, no. 23, pp. 5203–5216, Dec. 2004.

Sai Chun Tang (S'97–M'01–SM'11) was born in Hong Kong, in 1972. He received the B.Eng. degree (with First Class Hons.) and the Ph.D. degree in electronic engineering from the City University of Hong Kong, Kowloon Tong, Hong Kong, in 1997 and 2000, respectively, where he was a Research Fellow after he graduated.

He joined the National University of Ireland, Galway, as a Visiting Academic in 2001, and then the Laboratory for Electromagnetic and Electronic Systems, Massachusetts Institute of Technology, Cambridge, MA, USA, in 2002. Since 2004, he has been with the Radiology Department, Brigham and Women's Hospital, Harvard Medical School, Boston, MA, for the developments of ultrasound diagnosis devices and noninvasive treatment systems using high-intensity focused ultrasound. In 2008, he became a Faculty in Radiology at Harvard Medical School. His current research interests include wireless power transfer, electronic medical devices, high-frequency electromagnetism, low-profile power converter design, and analog electronics.

Nathan J. McDannold received the B.S. degree from the University of Virginia, Charlottesville, VA, USA, and the Ph.D. degree from Tufts University, Boston, MA, USA, both in physics, in 1995 and 2001, respectively.

He is the Research Director of the Focused Ultrasound Laboratory, The Brigham and Women's Hospital, Boston and an Associate Professor in radiology at Harvard Medical School, Boston. His work has been primarily concerned with the development and implementation of MRI-based thermometry methods, animal experiments testing MRI and ultrasound related work, and clinical focused ultrasound treatments of breast tumors, uterine fibroids, and brain tumors. In recent years, the main focus of his work has been studying the use of ultrasound for temporary disruption of the blood-brain barrier, which may allow for targeted drug delivery in the brain.

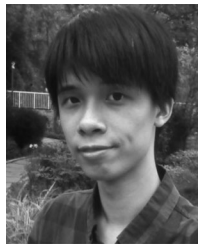

Tian Le Tim Lun received the B.Eng. degree in mechanical engineering from the University of Hong Kong, Hong Kong, in 2015, where he is currently working toward the M.Phil. degree.

His research interests include the design and sensing of soft robotics, medical, and surgical robotic devices.

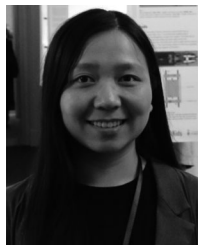

Ziyan Guo received the B.Eng. degree from the Department of Vehicle Engineering, Tsinghua University, Beijing, China, in 2013. She is currently working toward the Ph.D. degree at the University of Hong Kong, Hong Kong.

Her research interests include the designs on MRI-guided robotic interventions and intracardiac catheter interventions.

Ka-Wai Kwok received the Ph.D. degree from the Department of Computing, Imperial College London, London, U.K., in 2012.

He is currently an Assistant Professor in the Department of Mechanical Engineering, University of Hong Kong, Hong Kong. His research interests include the designs of medical and surgical robotic devices, as well as their control interface for endoscopy, laparoscopy, stereotactic, and intracardiac catheter interventions.

Dr. Kwok has been recognized by several awards from the IEEE international conferences, including ICRA'14, IROS'13, and FCCM'11. He also received Early Career Awards 2015/2016 offered by the Research Grants Council of Hong Kong.